Magnetism in the few-monolayers limit: A surface magneto-optic Kerr-effect study of the magnetic behavior of ultrathin films of Co, Ni, and Co-Ni alloys on Cu(100) and Cu(111)

F. Huang, M. T. Kief, G. J. Mankey, and R. F. Willis*
Department of Physics, The Pennsylvania State University, University Park, Pennsylvania 16802
(Received 28 July 1993; revised manuscript received 20 September 1993)

The surface magneto-optic Kerr effect (SMOKE) was used to investigate the magnetic properties of epitaxial thin films of Co, Ni, and their alloys grown on Cu(100) and Cu(111). The Curie temperature T_C is higher for the same films of a given thickness on Cu(111) than on Cu(100). All the films show a change in the power-law exponent β of the magnetization density $M \sim (1-T/T_C)^{\beta}$ with reducing film thickness. Ni films on Cu(100) undergo a particularly abrupt crossover at ~ 7 monolayers (ML) from three-dimensional Heisenberg ($\beta=0.37$) to finite-size two-dimensional XY ($\beta=0.23$) behavior as the film thickness is reduced. The characteristic power-law exponent $\beta=0.23$ of these films appears to be an experimental realization of Kosterlitz-Thouless behavior over a restricted temperature range. A similar, but more gradual crossover occurs for the Ni films on Cu(111) at 8 to 12 ML. The finite-size scaling behavior in the few-monolayers-thickness range is compared with that reported for Ising thin-film behavior. In all instances T_C extrapolates with decreasing thickness to zero at one monolayer. The dimensionality crossover and finite-size scaling behavior is discussed in the light of our current understanding of spin-wave quantization, anisotropy, and film microstructure.

INTRODUCTION

Magnetic thin films have unique properties that are not present in bulk materials due to reduced symmetry. These properties are sensitive to many local properties at the surface such as electronic band structure, crystallinity, and film morphology. In particular, these properties are sensitive functions of film thickness and growth conditions. This often leads to different, even contradictory, results from different groups working on the same system. Our goal in this paper is to report a complete and consistent set of measurements on model film-substrate systems which provide a coherent understanding of their magnetic behavior by varying the experimental conditions such as substrate symmetry, film thickness, magnetic alloy composition, and morphology. The sensitivity of the magnetic phase transition on these experimental parameters is of particular interest, due to the possibility of experimentally realizing two-dimensional (2D) behavior in the monolayer (ML) limit. Also, the results are pertinent to recent developments in oscillatory magnetic coupling and giant magnetoresistance in layered heterostructures which prompt potential applications in data storage technologies.

To study the thickness-dependent magnetic behavior, Ni is a good candidate since it has the lowest bulk Curie temperature ($T_C=627$ K) compared with Fe and Co. This allows experiments over a wide thickness range where the T_C of the thicker films begins to approach the bulk value. Also, fcc Ni films are generally more stable both structurally and magnetically, compared to fcc Fe, which exhibits complex magnetization reorientation behavior[1] with different magnetic phases depending on the lattice parameter in epitaxial thin layers.[2] Despite its relatively weak bulk magnetism, Ni films have been widely studied and show unusual behavior. For instance, a distinct dimensionality crossover in the critical behavior has been reported for Ni films grown on W(110).[3] These films display 2D Ising behavior ($\beta \cong 0.13$) below 5 ML changing to three-dimensional (3D) Heisenberg ($\beta \cong 0.37$) for thicker films. Earlier experiments reported a $\beta=0.24$ for ultrathin films of Ni on Cu(111) (Ref. 4) and $\beta=0.22$ for Fe films on Au(100).[5] These β values do not seem to belong to any universality class but are frequently reported in various thin films and layered compounds.[6] What the meaning of these values is and what factors determine the dimensionality crossover are the questions we would like to address in this paper.

Co and Ni are miscible and form stable alloys near room temperature.[7] By varying the Co content, we can produce stable alloy materials with different bulk T_C values. This provides supplementary systems to study the thickness dependence of the magnetic behavior. We choose Cu as the substrate since both Co and Ni films on Cu have been widely studied and are fairly well understood. Measurements on low-index surface with different symmetry provide new insight into the extraordinary magnetic behavior in the ultrathin-film regime.

In the following, we will present experimental results on the thickness-dependent magnetic phase-transition behavior of these films followed by a discussion of dimensionality crossover and finite-size scaling behavior in these ultrathin films. These properties are discussed in connection with the roles of magnetic anisotropy and strain-induced microstructural effects.

EXPERIMENT

Our vacuum system consists of two parts: a sample preparation chamber with molecular-beam epitaxy

(MBE), ion gun for sputtering, Auger electron spectroscopy (AES), low-energy electron diffraction (LEED), and reflection high-energy electron diffraction (RHEED); and the analysis chamber for the surface magneto-optic Kerr effect (SMOKE), thermal desorption spectroscopy (TDS), and angle-resolved ultraviolet photoemission spectroscopy (ARUPS) measurements. A long stroke sample manipulator traverses the central axis of the chambers. For easy access to different samples, a load lock was added to allow sample transfer to the main sample manipulator. The base pressure is lower than 2×10^{-10} mbar.

Particular attention has been paid to sample preparation since the quality of the substrate surface is a crucial factor for meaningful measurements. The crystals were cut and aligned along the [100] or [111] direction to within 0.5° using a Laue x-ray diffractometer. They were then mechanically polished down to 0.05 μm followed by electropolishing[8] to remove the mechanically damaged layers before introduction into the vacuum. After a few cycles of 500 eV Ar^+ sputtering and subsequent annealing at 700 K, the substrates were free of contamination as determined by AES and showed a sharp $p(1\times1)$ LEED pattern.

Co and Ni films were epitaxially grown on the single-crystal copper substrates at room temperature, which is the optimum growth temperature for good epitaxy without interdiffusion.[4,9,10] The flux rates were carefully controlled with calibrated quartz-crystal monitors to ensure uniform monolayer growth conditions. Film thickness was controlled by quartz-crystal monitors calibrated with RHEED oscillations. The alloy films were grown by simultaneously evaporating Co and Ni at proportionate rates, typically 0.6 ML/min. The Ni and Co-Ni alloy films were annealed at 450 K for a short time to further improve the smoothness of the films.

The magnetic properties were measured *in situ* using SMOKE with the arrangement shown in Fig. 1. A linearly polarized He-Ne laser was used as a light source. The laser light was further polarized by a linear polarizer, set to 0.2° from extinction in the plane of incidence, and incident on the film surface at ~70° off from the film surface normal. The reflected light went through a beam splitter, with beam separation of ±5° and an equivalent extinction ratio of 10^{-5}. The combination of the beam splitter and two photodiodes allows simultaneous detection of the two orthogonal light components. A four-pole electromagnet allows the external magnetic field to be applied either parallel (longitudinal) or perpendicular (polar) to the film plane.[11] The height of the hysteresis loops in remnant state ($H=0$) is referred to as the Kerr intensity. To study the magnetic phase transition, the Kerr intensity was measured as a function of substrate temperature, which was ramped at a constant rate of 6 K/min. The substrate temperature was measured by a type-*K* thermocouple, spot-welded to the supporting Mo plate of the sample holder. The temperature difference between the sample and the Mo plate was determined to be less than 5 K at the experimental heating rate of 6 K/min.

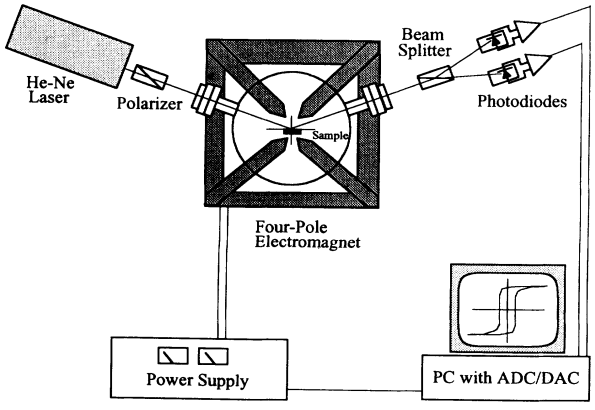

FIG. 1. Schematic diagram of the SMOKE apparatus.

RESULTS AND DISCUSSION

A. Film growth and characterization

Ni on Cu is a good epitaxial system since they both have the same fcc crystal structure with only 2.5% lattice mismatch. Ultrathin films of Ni form pseudomorphic layers which are strained to match the Cu substrate lattice until a critical thickness is reached.[12] Above this thickness, misfit dislocations occur as it is energetically more favorable to accommodate lattice mismatch by dislocations than by elastic strain. Transmission-electron-microscopy experiments have shown that the critical thickness for Ni on Cu(100) is 14.6 Å(~8 ML) (Ref. 13). On Cu(111), epitaxial growth of Ni proceeds up to 25 Å(~12 ML) as was estimated theoretically[14] and observed experimentally,[15,16] In addition, Ni on Cu is thermally stable against interdiffusion to cycling temperatures up to 490 K.[17] This is important since the widest possible range of temperature variation is required during the T_C measurements.

The growth of Co is more complicated than Ni since the equilibrium phase of bulk cobalt is hcp at room temperature and fcc at temperatures above 697 K.[18] It is possible that both phases are present during the film growth. However, Co films epitaxially grown on Cu(100) surfaces are formed in a stable fcc structure because no low-index orientation of the hcp structure matches the Cu(100) surface.[19–21] Angle-resolved x-ray photoemission scattering (ARXPS) results have shown that Co grows on Cu(100) in a well-ordered fcc structure via a layer-by-layer growth from 2 to 20 ML thickness. Below 2 ML, the growth is nearly layer-by-layer with the initial formation of two-layer-high islands.[21] This is consistent with our RHEED measurements as shown in Fig. 2(a). The first maximum in RHEED intensity is low, corresponding to island formation. After the completion of the second monolayer, the well-resolved oscillations indicate good layer-by-layer epitaxy. In sharp contrast, Co on Cu(111) does not show any RHEED oscillations, as has also been reported before.[22] This could be because both fcc(111) and hcp(0001) phases are present during growth with up to 50% hcp fraction.[23,24] Recent experimental results have shown that the first two layers of Co continue the fcc stacking

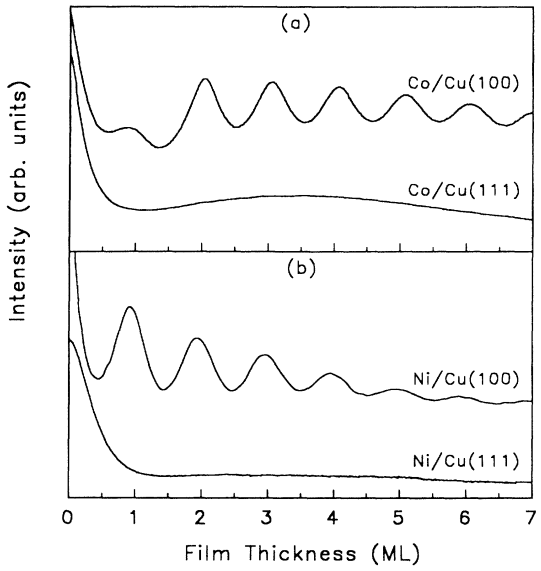

FIG. 2. RHEED oscillations for (a) Co, and (b) Ni on Cu(100) and Cu(111) substrates at room temperature. The electron-beam energy is 5 keV, incident angle is 3.5° and the azimuth is [100] for Cu(100) and [1$\bar{1}$0] for Cu(111). The evaporation rate is 0.6 ML/min.

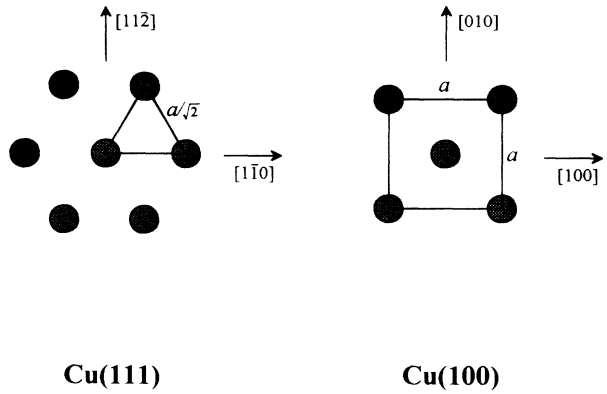

FIG. 3. Unit cells of the Cu(111) and Cu(100) surfaces. The atomic area density is $2/a^2$ ($1/\text{Å}^2$) on Cu(100) and $4/(\sqrt{3}a^2)$ on Cu(111), $a=3.61$ Å is the Cu lattice constant.

sequence through a layer-by-layer and pseudomorphic growth mode, and the hcp phase starts to develop in the third layer.[24] In this work, all of the Co films investigated have thicknesses below 2 ML so that the fcc structure is expected to be dominant. Particular attention was paid to avoid Cu segregation on top of the Co films during the annealing phase since interdiffusion occurs at a relatively low temperature of 450 K on the Cu(100) surface[9] and at the higher temperature of 550 K for carefully annealed Co films on Cu(111).[25]

A puzzling result is that there are no RHEED oscillations observed for Ni on Cu(111) [Fig. 2(b)], although it is expected to be a good epitaxial system. We have varied the film growth conditions, such as the substrate temperature during growth and evaporation rate, which can dramatically affect the growth mode,[26] but still without seeing any oscillations. One possible explanation is that Ni on Cu(111) has a higher volume deformation (3.8%) than on Cu(100) (2.2%).[16] This may lead to a textured layer structure. A more likely reason, however, could be that it is not a good layer-by-layer growth system. This is supported by the fact that Ni/Cu(111) shows a much more pronounced rounding and tailing of the magnetization curve near T_C than the Ni/Cu(100) films, as will be discussed in the next section. This tailing is due to finite-size effects[27] which provide a sensitive measure of the film microstructure such as island formation.[28,29] More detailed studies on the morphology of this particular system, Ni/Cu(111), are needed.

The absence of RHEED oscillations for both Co and Ni on Cu(111) presents a difficulty for a direct thickness calibration. Instead of using the Auger break method,[30] which usually has an error $>10\%$, we use the well-resolved RHEED oscillations on Cu(100) to calibrate the evaporator flux. Since, as shown in Fig. 3, the atomic area density is $2/a^2$ for Cu(100) and $4/(\sqrt{3}a^2)$ for Cu(111), one monolayer on Cu(100) covers only $2/(4/\sqrt{3})=86.6\%$ of the Cu(111) surface. Therefore, the thickness on Cu(111) is 86.6% of that on Cu(100), given the same amount of deposited material.

B. Magnetic phase transition

The magnetic properties of thin films can deviate significantly from their bulk behavior when the film thickness is reduced to atomic scale due to broken symmetry in the direction perpendicular to the film plane. In particular, the Curie temperature T_C that signifies zero magnetization and separates the ferromagnetic and paramagnetic phases, decreases with decreasing thickness according to finite-size scaling theory considerations.[31] T_C is determined from the phenomenological power-law fits to the data, $M(T)=M_0(1-T/T_C)^{\beta}$, where M is the magnetization proportional to the Kerr intensity and β is a power-law exponent characterizing the magnetic ordering behavior. Figure 4 shows sample $M(T)$ curves for different systems: Ni/Cu(100), Ni/Cu(111), and Co_1Ni_9/Cu(100). In all the curves, the magnetization extends above the estimated T_C due to finite-size magnetic spin-correlation effects. Ni films on Cu(100) show the sharpest phase-transition behavior with tailing less than 5%, indicating very good surface and film quality. In contrast, similarly prepared alloy films of Co_1Ni_9 show a significantly longer tail indicative of magnetic or compositional inhomogeneities. Ni films on Cu(111) exhibit more prominent tailing than on Cu(100) which suggests less structural homogeneity. This observation is supported by the absence of RHEED oscillations which argues a case for the (111) films not being uniform in thickness on an atomic scale.

All of these films display a clear monotonic thickness dependence of T_C, as illustrated in Fig. 5 for Co, Ni, and Co_xNi_{1-x} alloy films on Cu(100). An interesting observation is that T_C extrapolates to zero at about 1 ML in all cases[10] as we have reported for another system, Co_xCu_{1-x} on Cu(100).[32] The disappearance of ferromagnetic long-range order approaching the monolayer re-

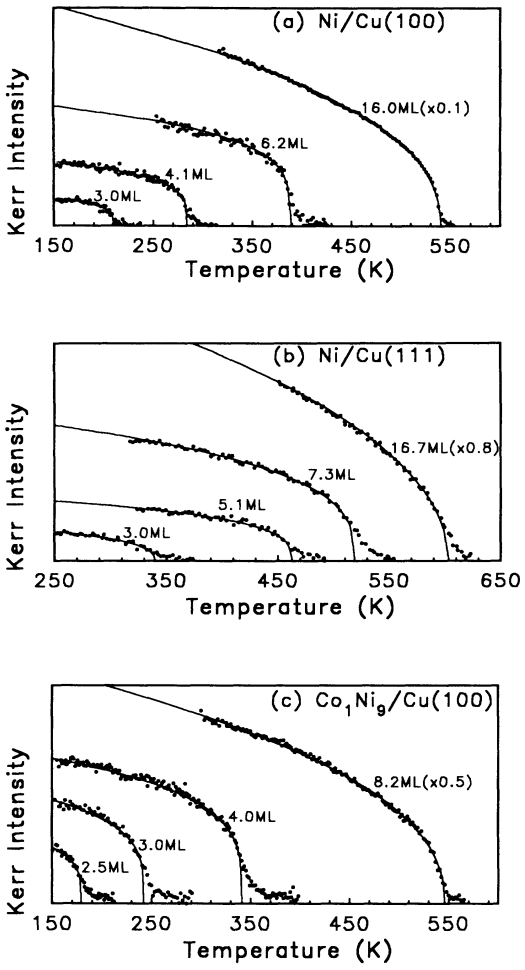

FIG. 4. Kerr intensity vs temperature at different thicknesses for (a) Ni/Cu(100), (b) Ni/Cu(111), and (c) Co_1Ni_9/Cu(100). The 16.0 ML Ni(100) curve is taken from polar hysteresis loops and all others are longitudinal. The solid lines are power-law fits to $M=M_0(1-T/T_c)^{\beta}$.

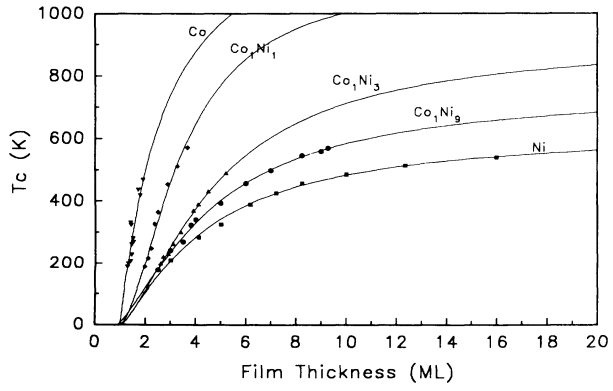

FIG. 5. Thickness dependence of T_C for Co-Ni alloy films with different compositions on Cu(100). The solid lines are finite-size scaling fits to Eq. (2) in text.

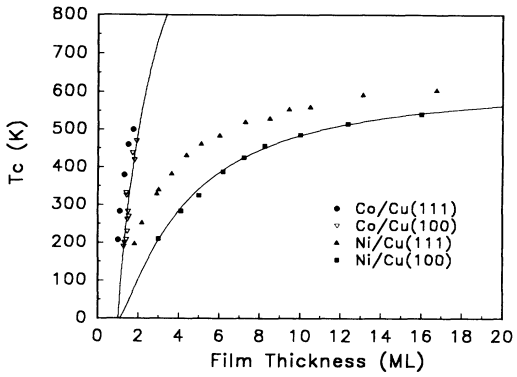

FIG. 6. Thickness-dependent T_C curves showing that both Co and Ni films have higher transition temperatures on Cu(111) than on Cu(100). The solid lines are finite-size scaling fits to Eq. (2).

gime appears to be system independent. All of the curves shown (Fig. 5) obey the same scaling-law relationship.[10]

In Fig. 6, we compare this thickness dependence of T_C for the films on Cu(111) and Cu(100). Both Co and Ni films display a higher T_C on Cu(111) than on Cu(100). The Curie temperature of thin films depends on many quantities such as magnetic anisotropy, exchange coupling, and electronic band structure.[33] All of these quantities can be easily changed by surface symmetry and lattice mismatch-induced strain. Using a generalized mean-field theory, the authors in Ref. 33 obtained a higher T_C on the (111) surface than on the (100) surface, in agreement with our experimental results. In fact, many (111) textured films with a strong uniaxial anisotropy show a distinctively higher T_C than the (100) textured films with planar anisotropy, which is consistent with the theoretical arguments[34] and these experimental results. What is surprising is the similar monotonic behavior extrapolating to $T_C=0$ in the monolayer limit.

C. Anisotropy

All of the Co, Ni, and Co-Ni alloy films grown on Cu(100) surface (Fig. 5) display a strong in-plane anisotropy in agreement with theoretical predictions[35] and previous experimental results.[11,20,36,37] Ni is an exception in that, as the thickness increases above 7 ML, a perpendicular component of the magnetization begins to develop, as indicated by the Kerr signal hysteresis loops [Fig. 7]. The in-plane component stays nearly the same while the coercivity increases rapidly and beyond our maximum magnetic field ($\sim$150 Oe) at 16 ML. This indicates that the magnetization is oriented parallel to the film plane for films below 7 ML and rotates out-of-plane for thicker films. The presence of both components of magnetization could be due to a canted single-domain state, or due to a statistical distribution of in-plane and out-of-plane multidomain state. The possibility of a canted spin state is excluded since the polar loops have 100% remanence. Therefore, we believe that perpendicular magnetization dominates at thickness above 7 ML, and the fraction of the perpendicular domains increases with increasing

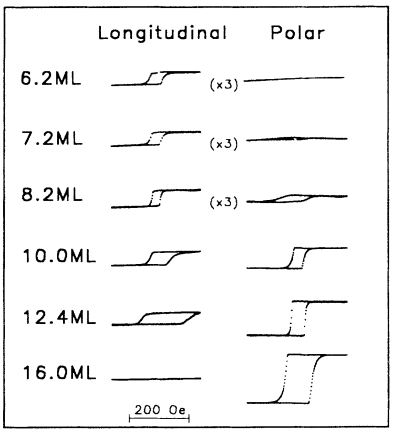

FIG. 7. Hysteresis loops of Ni films on Cu(100) showing the spin reorientation at around 7 ML. All the loops are measured at 160 K.

thickness.[32] Since Co has a much stronger in-plane anisotropy to begin with, the magnetization remains in plane over the whole thickness range [$n \leq 9$ ML for Co-Ni alloys[32] and $n \leq 15$ ML for Co (Ref. 20)].

Both Co and Ni on Cu(111) show mainly in-plane anisotropy, but a weak perpendicular magnetization with a significantly larger coercivity is always present in the as-grown films. This is consistent with previous experimental reports on these systems.[23,38] The [111] direction is the easy axis for both bulk fcc Co and Ni. Thin films of Co grown on fcc(111) surfaces have a much stronger perpendicular anisotropy than those on (100) surfaces due to this magnetocrystalline anisotropy. This has been observed in the Co on Pd system where a spin reorientation from perpendicular to in-plane magnetization occurs below about 1 to 2 ML on Pd(100) and 6 ML on Pd(111).[39,40] This reorientation of the magnetization is determined by the two competing anisotropies: surface anisotropy which favors perpendicular orientation and dominates in the ultrathin regime, and shape anisotropy that favors in-plane orientation which can overcome the surface anisotropy as film thickness increases.[35]

A demonstration of the importance of interface effects is shown by coating the Co films grown on Cu(100) and Cu(111) surfaces with a few monolayers of Cu. As-grown Co films have both perpendicular and in-plane components of the magnetization. However, on coating with just 2 ML of Cu, the Co/Cu(111) film shows a remarkably enhanced perpendicular anisotropy while the in-plane anisotropy appears to collapse, as shown by the hysteresis loops in Fig. 8(a). In contrast, the Co/Cu(100) film remains unaffected [Fig. 8(b)].

The incidence of enhanced perpendicular magnetization may also be indicative of a different micromorphology for films on Cu(111). Roughness and lattice mismatch-induced strains are known to induce a modified magnetocrystalline and magnetoelastic surface anisotropy.[41]

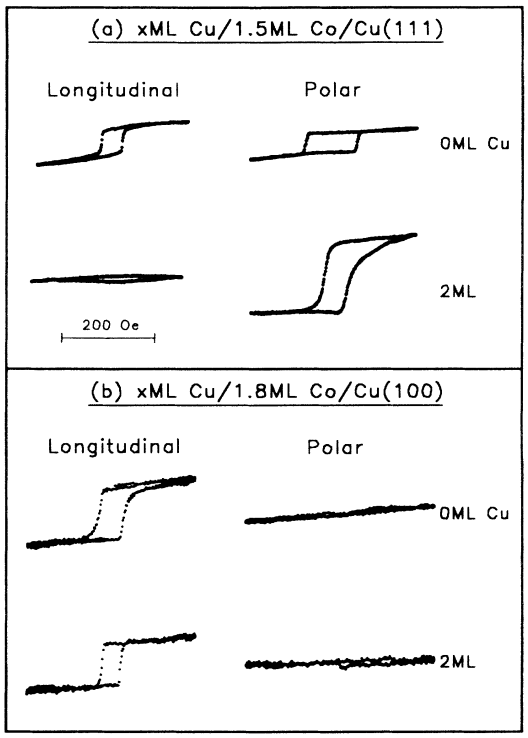

FIG. 8. Hysteresis loops showing the effect of Cu capping on magnetic anisotropy: (a) dramatic enhancement of the perpendicular anisotropy for Co/Cu(111) and (b) only a small reduction on the longitudinal loop for Co/Cu(100).

D. Crossover from 3D to 2D behavior

We extract T_C and β using the standard methodology as outlined by Dürr *et al.*[5] and assume a power-law behavior $M \sim (1-T/T_C)^{\beta}$ for the magnetization as a function of temperature. The exponent β is deduced by choosing a T_C value that maximizes the linear range in the $\log_{10}(M)$ versus $\log_{10}(1-T/T_C)$ plot.[42] Such log-log plots are shown in Fig. 9 for Ni films on Cu(100). The β values obtained from the slopes of the straight-line fits are 0.43 for 16 ML Ni and 0.23 for thin films below 7 ML. Values for Ni/Cu(100), Ni/Cu(111), and Co/Cu(111) are summarized in Table I. In Fig. 10, we show the thickness dependence of β values for Ni/Cu(100) and Ni/Cu(111) and compare them with published results for Ni(111)/W(110) from Ref. 3.

A distinct jump in β values is seen at the thickness of 7 ML for Ni on Cu(100) [Fig. 10(a)]. Above this thickness, the β values range from 0.38 to 0.43. We note that $\beta=0.37$ is characteristic of a 3D Heisenberg spin-lattice system[43] and $\beta=0.42$ is the experimental value for bulk Ni.[44] Below 7 ML, all the films show $\beta \approx 0.23$, which we believe to be a typical behavior of a finite-size 2D XY system.[6] This will be discussed in more detail in the next section. The sudden change in β values at 7 ML indicates a dimensionality crossover from 3D Heisenberg to 2D XY behavior. A similar but more gradual crossover has also been reported in Ni(111) films on W(110) (Ref. 3) and is shown in Fig. 10(c). In this case, a gradual change from

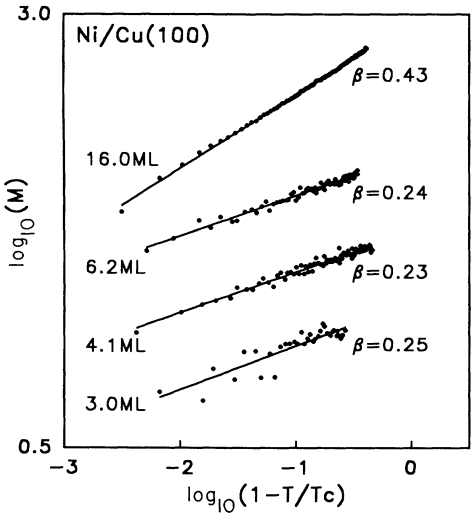

FIG. 9. $\text{Log}_{10}(M)$ vs $\log_{10}(1-T/T_C)$ plots for the Ni/Cu(100) data from Fig. 4(a) showing the thickness dependence of the β values. The data sets are offset for clarity.

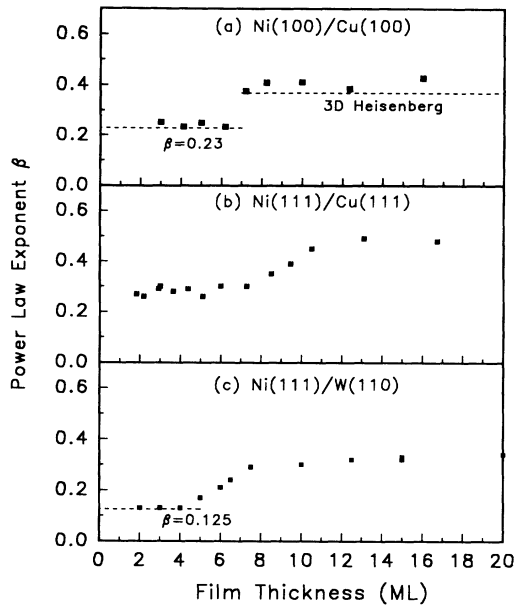

FIG. 10. Power-law exponent β vs film thickness showing dimensional crossover for (a) Ni/Cu(100), (b) Ni/Cu(111), and (c) Ni(111)/W(110). The Ni(111)/W(110) data are from Ref. 3. The dashed lines are theoretical values for 2D Ising ($\beta=0.125$), finite-size 2D XY ($\beta=0.23$) and 3D Heisenberg ($\beta=0.37$) models.

3D Heisenberg to 3D Ising at large thicknesses is followed by a drastic crossover from 3D Ising to 2D Ising in the thickness range between 5 to 7 ML. The uniaxial Ising behavior arises from the strong in-plane, strain-induced anisotropy due to a large lattice mismatch along the $[1\bar{1}0]$ direction of the fcc Ni(111) films on bcc W(110).

Ni films on Cu(111) [Fig. 10(b)], on the other hand, also show a gradual change in β values from 0.49 to 0.26 in the thickness range from 8 to 12 ML. The uncertainty in these β values is larger than those of the Ni/Cu(100) system because the magnetization is not so accurately described by the phenomenological power law. The presence of both perpendicular and in-plane components of magnetization, and the more pronounced finite-size tailing near T_C makes β more difficult to quantify (Table I). We identify the large β values above 12 ML as typical of bulk Ni behavior. Given these uncertainties, $\beta\sim0.26$ for films less than 8 ML thick is in the range of the finite-size 2D XY behavior characteristic of the Ni/Cu(100) system. A β value of 0.24 ± 0.07 has been previously reported for similar ultrathin Ni films on Cu(111),[4] in agreement with our measurements.

An ultrathin film can be considered magnetically 2D if spin waves with wave vector K normal to the film plane cannot be excited. The normal component of the spin-wave vector is quantized in discrete amounts

TABLE I. Experimental values of transition temperature T_C and power-law exponent β for three different systems: Ni/Cu(100), Ni/Cu(111), and Co/Cu(111). The estimated errors for β are included based upon the noise level, finite-size rounding, and interdiffusion effects.

Ni/Cu(100)			Ni/Cu(111)			Co/Cu(111)		
n (ML)	β	T_C (K)	n (ML)	β	T_C (K)	n (ML)	β	T_C (K)
3.0	0.25(6)	210	1.8	0.27(7)	197	1.0	0.17(9)	207
4.1	0.23(5)	284	2.2	0.26(7)	253	1.1	0.27(9)	283
5.0	0.25(5)	325	2.9	0.29(7)	329	1.3	0.30(9)	380
6.2	0.24(5)	388	3.0	0.30(7)	340	1.5	0.15(8)	460
7.2	0.38(4)	425	3.6	0.28(7)	382	1.7	0.15(8)	500
8.2	0.41(4)	456	4.4	0.29(7)	431			
10.0	0.41(4)	485	5.1	0.26(7)	462			
12.4	0.39(4)	514	6.0	0.30(7)	483			
16.0	0.43(4)	540	7.3	0.30(7)	519			
			8.5	0.35(6)	529			
			9.5	0.39(6)	554			
			10.5	0.45(8)	559			
			13.1	0.49(8)	591			
			16.7	0.48(8)	603			

$K_\perp = (m\pi/na_0)$, $m = 1,2,\ldots$ for a film n layers thick and lattice constant a_0. At the crossover thickness, only the lowest $m = 1$ spin-wave branch is thermally populated. As the film thickness decreases to below this critical thickness, spin fluctuations propagating in the normal direction are "frozen out" and the films display the thermodynamic properties of a 2D system. The 2D nature of the phase transition is also seen from the thickness independence of β values in the ultrathin region, as shown in Fig. 10. A similar invariance of the β values in the 2D regime has been previously reported for 1 to 2.5 ML Fe films on Au(100) (Ref. 5) and the Ising-like Ni films on W(110) below 4 ML thick.[3] In this 2D regime, the correlation length is too small for any magnetic fluctuations normal to the film to be relevant.[6] This quantization of excitations is a general characteristic of thin-film structures. Recent photoemission experiments[45] have shown that the quantization of electronic fluctuations about the Fermi level E_F propagating in the perpendicular direction, results in discrete quantum-well states, with a periodicity of ~ 6 ML. This value is close to that observed in Fig. 10 at which a sudden crossover from 3D to 2D behavior occurs. It is also a number that relates to the periodicity of oscillatory magnetic coupling observed in magnetic superlattices and sandwich systems.[46]

While spin-wave vector quantization is the determinant factor, the actual crossover thickness value is affected by the microstructure of the films. Comparing the three systems Ni on Cu(100), Cu(111), and W(110), observe that dimensionality crossover in magnetic power-law behavior is also associated strongly with a film structural change from a strained two-dimensional pseudomorphic film to a three-dimensional bulklike film in which strain is relaxed by the formation of misfit dislocations. Both dimensionality crossover and this structural change occurs at ~ 7 ML for Ni/Cu(100) [Fig. 10(a), Ref. 13], and ~ 12 ML for Ni/Cu(111) [Fig. 10(b), Refs. 14–16]. The crossover for the fcc Ni(111) films on bcc W(110) occurs at a relatively smaller thickness (5 to 7 ML) because there is a larger strain along the $[1\bar{1}0]$ direction. These strains affect the electronic band structure and, particularly, the wave vectors of the electronic fluctuations about E_F, that ultimately sanction the overall magnetic behavior.

It is interesting to note that the anisotropy itself is not playing the pivotal role in determining dimensionality crossover. Although Ni/Cu(100) has both spin reorientation and dimensional crossover at ~ 7 ML, the other systems investigated show no correlation between these two phenomena. Co_1Ni_9 films showed the same jump in β values at 7 ML but no change in anisotropy is observed in the Kerr hysteresis loops, remaining always in-plane for all the thicknesses studied ($n < 9$ ML).[32] Likewise, Ni/Cu(111) does not show any sign of change in anisotropy near the crossover thickness of 8 to 12 ML. Similarly, the reported crossover behavior of Ni(111)/W(110) (Ref. 3) shows no change in anisotropy.

E. Finite-size 2D XY behavior

In the previous section, we identified the $\beta = 0.23$ as being characteristic of finite-size 2D XY behavior. An infinite isotropic 2D XY system cannot sustain long-range order,[47] but, nevertheless, exhibits a Kosterlitz-Thouless phase transition involving the unbinding of spin vortices at a critical temperature T_{KT}.[48] This thermodynamic limit, however, is hardly accessible in most experimental systems. In real materials, there are many factors such as anisotropy,[34,49] finite size,[6] and interlayer coupling[28] that can stabilize the spontaneous order. Recent renormalization-group analysis[6] has shown that a 2D XY spin lattice of a finite size can develop finite magnetization which approaches power-law behavior over a restricted temperature range, around the Kosterlitz-Thouless critical temperature T_{KT}, with an effective exponent $\beta = 0.23$. Layered Heisenberg ferromagnets of finite size with planar anisotropy can also be considered as experimental realization of this 2D XY model. We believe that our thin transition-metal films are the analog to such systems.

In a finite-size 2D XY spin-lattice model, the slow decay of spin correlations can always ensure a finite magnetization.[50] Renomalized spin-wave theory[50–52] applied to a 2D lattice of N spins gives for the net magnetization at low temperature,

$$M(N,T) = \left\langle \left| \frac{1}{N} \sum_{i=1}^{N} \mathbf{S}_i \right| \right\rangle = \left[\frac{1}{2N} \right]^{1/8\pi D}, \tag{1}$$

where $D = J/k_B T$ is the effective spin-wave stiffness and J is the exchange coupling. A theoretical curve obtained from a Monte Carlo simulation of a 2D lattice of $N = 10^4$ spins[6] is compared with our experimental data for Ni on Cu(100) for thicknesses 4.1 and 6.2 ML in Fig. 11. The experimental data has a much shorter tail, indicating our films have a spin domain size larger than $N = 10^4$ spins. We estimate the domain size to be around 0.5 μm, which corresponds to $N \sim 10^6$ spins.

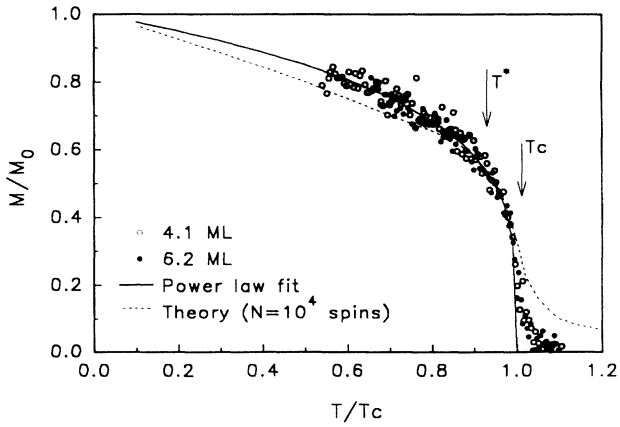

FIG. 11. Magnetization curves showing $\beta = 0.23$ power-law behavior for the 4.1 and 6.2 ML of Ni films on Cu(100). The full curve is the power-law fit to data. The dashed curve is the result of a Monte Carlo simulation on a 2D XY spin lattice with $N = 10^4$ spins (Ref. 6). T^* is the shifted Kosterlitz-Thouless transition temperature and T_C represents the onset of magnetization. Note the good agreement near T^*.

The renormalization-group theory analysis[6] predicts $\beta=3\pi^2/128=0.23$ at T^*, where T^* is the temperature below T_C at which $D=2/\pi$ and T_C is the temperature at which the spin-correlation length is equal to the system size. We note the good agreement between this theoretical value of T_C and the value from our power-law fit (full curve, Fig. 11). This β value is a characteristic of finite-size behavior at the shifted Kosterlitz-Thouless temperature T^*, but the range of temperature over which M follows this power-law behavior is not universal. It depends on the specific spin model. Our experimental data are representative of a finite-size 2D XY system perturbed by a weak interlayer exchange coupling. The magnetization fits a power-law behavior with $\beta=0.23$ over a wider temperature range, from 0.6 to 1.0 T_C, than that predicted by the finite-size spin-lattice 2D mesh analysis.[6]

Figure 12 compares the normalized T_C behavior of all of our finite-size 2D XY ($\beta=0.23$) thin-film systems magnetized in-plane with published data on similar thin films exhibiting Ising behavior ($\beta=0.125$) viz. Fe(110)/Ag(111),[53] Ni(111)/W(110),[3] and Ni(111)/Re(0001).[54] T_C is significantly higher in the Ising films compared with the finite-size 2D XY films due to their strong uniaxial anisotropy. The results (Fig. 12) clearly distinguish two classes of behavior: type-I Ising behavior with a dimensionality crossover to $\beta=0.125$ and type-II 2D XY behavior with a dimensionality crossover to $\beta=0.23$. Both curves extrapolate to $T_C=0$ at one monolayer.

F. Finite-size scaling

Figures 5, 6, and 12 summarize the finite-size scaling properties of these two types of behavior: finite-size 2D XY films with $\beta=0.23$ and 2D Ising films with strong interfacial anisotropy with $\beta=0.125$. In a previous paper,[10] we have proposed that the Ni and Co films grown on Cu(100), and their alloys, obey a thickness-dependent scaling law of the form

$$\frac{1}{T_C(n)}=\frac{1}{T_C(\infty)}=\frac{1}{T_C(\infty)}\left[\frac{n-n'}{n_0}\right]^{-\lambda}. \quad (2)$$

That is, this monotonic relationship describes all of the films shown in Figs. 5, 6, and 12. Table II is a summary of the various best-fit parameters appropriate to each film. The most intriguing result is that all of the data extrapolate to $T_C=0$ in the monolayer limit.

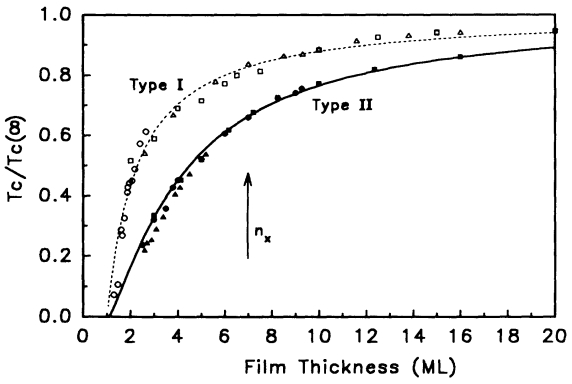

FIG. 12. Normalized T_C vs film thickness showing the influence of anisotropy on T_C. Type I films have strong uniaxial anisotropy ($\beta=0.125$) and higher T_C [Fe(110)/Ag(111) from Ref. 53 (○), Ni(111)/W(110) from Ref. 3 (□), Ni(111)/Re(0001) from Ref. 54 (△)] compared with the type-II films ($\beta=0.23$) [Ni (■), Co_1Ni_9 (●), and Co_1Ni_3 (▲) on Cu(100) from this work]. n_x represents the thickness at which crossover occurs from 3D to 2D behavior.

TABLE II. Finite-size scaling parameters determined by the thickness-dependent T_C behavior. Experimental errors are included in Ni and Co_1Ni_9 films. Due to the narrow thickness range for the Co_1Ni_3, Co_1Ni_1, and Co films, data are fitted to the scaling law with a fixed value $n'=1.0$ ML.

Films/Cu(100)	λ	n' (ML)	n_0 (ML)
Ni	1.25(7)	1.1(2)	3.4(2)
Co_1Ni_9	1.39(8)	0.9(2)	3.7(2)
Co_1Ni_3	1.49	1.0	3.8
Co_1Ni_1	1.66	1.0	2.5
Co(Ref. 11)	1.02	1.0	1.8

Although it is tempting to identify this with the well-known Mermin-Wagner limit,[47] this would imply that the magnetic order parameter is isotropic with infinite long-range order in-plane. However, as the films approach the monolayer limit, it is possible that they are no longer homogeneous and uniformly thick layers, but begin to break up into islands of varying thickness. The behavior could then tend toward superparamagnetic behavior, although we have seen no evidence for such behavior to date. An alternative explanation is that it is the electronic properties which are changing, and changing in such a way that the ferromagnetic exchange splitting of the states is decreasing rapidly to zero. Again, however, we have no photoemission evidence to date to support this.[55] Finally, recent measurements of the magnetic anisotropy[56] indicate that the volume and surface anisotropy constants are rapidly decaying to zero as the monolayer limit is approached. This would support a 2D isotropic ordering parameter picture. What is intriguing is that a wide variety of these transition-metal ferromagnetic thin-film systems exhibit such similar behavior in the monolayer limit, whether Ising-like (type-I) or 2D XY (type-II) (Fig. 12).

CONCLUDING REMARKS

We have grown high-quality thin films of Co, Ni, and their alloys on Cu single crystals with different symmetry surface meshes: Cu(100) and Cu(111). These films display very similar magnetic power-law behavior which changes at a critical thickness signifying crossover from 3D to 2D. The main conclusions to be drawn from these experiments are as follows:

(i) Both Co and Ni can grow on Cu(100) in a well-ordered fcc structure via a layer-by-layer growth mode. However, the growth on the Cu(111) surface may be characterized by island formation and different crystal

phases judging from the large finite-size rounding and the absence of RHEED oscillations.

(ii) T_C is higher on the (111) surface than on the (100) surface for a given film thickness.

(iii) For Ni/Cu(100), the magnetization lies in-plane at thicknesses $<7ML$ and cants out-of-plane above 7 ML. All of the Co ($n<2$ ML) and Co-Ni alloy films ($n<9$ ML) on Cu(100) have only in-plane magnetization. The Co and Ni films on Cu(111) show a predominantly in-plane anisotropy, but a weak perpendicular magnetization with a large coercivity is always present at all thicknesses considered.

(iv) Cu capping can drastically enhance the perpendicular anisotropy on the Cu(111) surface.

(v) Ni and Co-Ni alloy films on Cu(100) undergo an abrupt dimensionality crossover at ~ 7 ML from 3D Heisenberg to finite-size 2D XY behavior. A similar, but more gradual crossover is found in Ni/Cu(111) at around 8 to 12 ML.

(vi) Dimensionality crossover is complicated by a film structural change. Below this critical thickness, the films are pseudomorphic and exhibit 2D magnetization power-law behavior. Above this thickness, films relax to reduce the epitaxial strain and the bulk magnetic properties are observed. The critical thickness is ~ 7 ML for Ni/Cu(100) and ~ 12 ML for Ni/Cu(111).

(vii) Dimensionality crossover appears to be independent of the nature of any magnetic anisotropy; both the Ising and 2D XY films show this effect occurring at several monolayers thickness.

(viii) $\beta=0.23$ is a general signature of a finite-size 2D XY system and an experimental realization of possible Kosterlitz-Thouless behavior. A magnetic phase transition is observed and follows the predicted power-law behavior over a wide temperature range below T_C.

(ix) The 2D XY (type-II) films all obey the same universal finite-size scaling law, with parameters distinct from those characteristics of 2D Ising (type-I) behavior.

(x) Strong uniaxial anisotropy results in a higher T_C for equivalent films of a given thickness.

(xi) T_C extrapolates to zero in the monolayer film-thickness limit for all of these films.

(xii) The indications are that the anisotropy, both surface and volume constants, rapidly decay to zero as the monolayer limit is approached. The exact mechanism is not understood.

ACKNOWLEDGMENTS

This work was supported by National Science Foundation Grant No. DMR 9121736. We would like to thank Steve Bramwell and Peter Holdsworth for their stimulating interactions and valuable correspondence.

*Author to whom correspondence should be addressed.

[1]J. Thomassen, F. May. B. Feldmann, M. Wuttig, and H. Ibach, Phys. Rev. Lett. **69**, 3831 (1992); Z. Q. Qiu, J. Pearson, and S. D. Bader, *ibid.* **70**, 1006 (1993); D. P. Pappas, K.-P. Kamper, and H. Hopster, *ibid.* **64**, 3179 (1990); D. P. Pappas, C. R. Brundle, and H. Hopster, Phys. Rev. B **45**, 8169 (1992).

[2]V. L. Moruzzi, P. M. Marcus, K. Schwartz, and P. Mohn, Phys. Rev. B **34**, 1784 (1986); C. S. Wang, B. M. Klein, and H. Krakauer, Phys. Rev. Lett. **54**, 1852 (1985); F. J. Pinski, J. Staunton, B. L. Gyorffy, D. D. Johnson, and G. M. Stock, *ibid.* **56**, 2096 (1986); W. Schwarzacher, W. Allison, R. F. Willis, J. Penfold, R. C. Ward, I. Jacob, and W. F. Egelholff, Jr., Solid State Commun. **71**, 563 (1989).

[3]Yi Li and K. Baberschke, Phys. Rev. Lett. **68**, 1208 (1992).

[4]C. A. Ballentine, R. L. Fink, J. Araya-Pochet, and J. L. Erskine, Phys. Rev. B **41**, 2631 (1990).

[5]W. Dürr, M. Taborelli, O. Paul, R. Germar, W. Gudat, D. Pescia, and M. Landolt, Phys. Rev. Lett. **62**, 206 (1989).

[6]S. T. Bramwell and P. C. W. Holdsworth, J. Phys. Condens. Matter **5**, L53 (1993); S. T. Bramwell and P. C. W. Holdsworth, J. Appl. Phys. **73**, 6096 (1993).

[7]H. Masumoto, Sci. Rep. Tohoku Univ., Ser. 1 **15**, 463 (1926), and references therein.

[8]W. J. M. Tegart, *The Electrolytic and Chemical Polishing of Metals in Research and Industry*, 2nd Rev. ed. (Pergamon, New York, 1959).

[9]G. J. Mankey, M. T. Kief, and R. F. Willis, J. Vac. Sci. Technol. **A7**, 1595 (1991).

[10]F. Huang, G. J. Mankey, M. T. Kief, and R. F. Willis, J. Appl. Phys. **73**, 6760 (1993).

[11]M. T. Kief, Ph. D. thesis, Pennsylvania State University, 1991.

[12]C. A. Haque and H. E. Farnsworth, Surf. Sci. **4**, 195 (1966); U. Gradmann, *ibid*, **13**, 498 (1969); R. Kuntze, A. Chambers, and M. Prutton, Thin Solid Films **4**, 47 (1969); M. A. Abu-Joudeh, B. M. Davies, and P. A. Montano, Surf. Sci. **171**, 331 (1986).

[13]J. W. Matthews and J. L. Crawford, Thin Solid Films **5**, 187 (1970).

[14]U. Gradmann, Ann. Phys. (Leipzig) **17**, 91 (1966).

[15]M. T. Johnson, J. J. de Vries, N. W. E. McGee, J. aan de Stegge, and F. J. A. den Broeder, Phys. Rev. Lett. **69**, 3575 (1992).

[16]David W. Gidley, Phys. Rev. Lett. **62**, 811 (1989).

[17]Y. Chen, S. T. Tong, J. S. Kim, M. H. Mohamed, and L. L. Kesmodel, Phys. Rev. B **43**, 6788 (1991); M. H. Mohamed, J. S. Kim, and L. L. Kesmodel, *ibid.* **40**, 1305 (1989).

[18]T. Nishizawa and K. Ishida, Bull. Alloy Phase Diagrams **4**, 387 (1983).

[19]A. Clarke, G. Jennings, R. F. Willis, P. J. Rous, and J. B. Pendry, Surf. Sci. **187**, 327 (1987).

[20]C. M. Schneider, P. Bressler, P. Schuster, J. Kirschner, J. J. de Miguel, and R. Miranda, Phys. Rev. Lett. **64**, 1059 (1990).

[21]Hong Li and B. P. Tonner, Surf. Sci. **237**, 141 (1990).

[22]Z. Q. Qiu, J. Pearson, and S. D. Bader, Phys. Rev. B **46**, 8195 (1992).

[23]M. T. Kief and W. F. Egelhoff, Jr., J. Appl. Phys. **73**, 6195 (1993).

[24]B. P. Tonner, Z. L. Han, and J. Zhang, Phys. Rev. B **47**, 9723 (1993).

[25]Qibiao Chen, M. Onellion, and A. Wall, Thin Solid Films **196**, 103 (1991).

[26]R. Kunkel, B. Poelsema, L. K. Verheij, and G. Comsa, Phys. Rev. Lett. **65**, 733 (1990).
[27]M. E. Fisher and A. E. Ferdinand, Phys. Rev. Lett. **19**, 169 (1967); D. S. Ritchie and M. E. Fisher, Phys. Rev. B **7**, 480 (1973); D. P. Landau, *ibid.* **13**, 2997 (1976).
[28]K. Hirakawa and K. Ubukoshi, J. Phys. Soc. Jpn. **50**, 1909 (1981); M. Donath, D. Scholl, H. C. Siegmann, and E. Kay, Phys. Rev. B **43**, 3164 (1991).
[29]G. Lugert and G. Bayreuther, Phys. Rev. B **38**, 11 068 (1988).
[30]W. Kirstein, B. Kruger, and F. Thieme, Surf. Sci. **176**, 505 (1986); K. H. Frank, R. Dudde, H. J. Sagner, and W. Eberhardt, Phys. Rev. B **39**, 940 (1989).
[31]A. E. Ferdinand and M. E. Fisher, Phys. Rev. **185**, 832 (1969); G. A. T. Allan, Phys. Rev. B **1**, 352 (1970); M. E. Fisher and M. N. Barber, Phys. Rev. Lett. **28**, 1516 (1972); K. Binder and P. C. Hohenberg, Phys. Rev. B **9**, 2194 (1974).
[32]F. Huang, M. T. Kief, G. J. Mankey, and R. F. Willis (unpublished).
[33]P. J. Jensen, H. Dreysse, and K. H. Bennemann, Surf. Sci. **169-270**, 627 (1992).
[34]M. Bander and D. L. Mills, Phys. Rev. B **38**, 12 015 (1988); R. P. Erickson and D. L. Mills, *ibid.* **43**, 11 527 (1991).
[35]J. G. Gay and R. Richter, Phys. Rev. Lett. **56**, 2728 (1986).
[36]H. P. Oepen, M. Benning, H. Ibach, C. M. Schneider, and J. Kirschner, J. Magn. Magn. Mater. **86**, L137 (1990).
[37]L. R. Sill, M. B. Brodsky, S. Bowen, and H. C. Hamaker, J. Appl. Phys. **57**, 3663 (1985).
[38]C. A. Ballentine, R. L. Fink, J. Araya-Pochet, and J. L. Erskine, Appl. Phys. A **49**, 459 (1989).
[39]F. J. A. den Broeder, D. Kuiper, H. C. Donkersloot, and W. Hoving, Appl. Phys. A **49**, 507 (1989).
[40]Brad N. Engel, Craig D. England, Robert A. Van Leeuwen, Michael H. Wiedmann, and Charles M. Falco, Phys. Rev. Lett. **67**, 1910 (1991).
[41]P. Bruno and J. P. Renard, Appl. Phys. A **49**, 499 (1989).
[42]D. L. Connelly, J. S. Loomis, and D. E. Mapother, Phys. Rev. B **3**, 924 (1971); R. M. Suter and C. Hohenemser, J. Appl. Phys. **50**, 1814 (1979).
[43]M. N. Barber, in *Phase Transitions and Critical Phenomena,* edited by C. Domb and J. L. Lebowitz (Academic, New York, 1983), Vol. 8; S. S. C. Burnett and Solomon Gartenhaus, Phys. Rev. B **43**, 591 (1991).
[44]C. Kittel, *Introduction to Solid State Physics,* 6th ed. (Wiley, New York, 1986), p. 425.
[45]J. E. Ortega, F. J. Himpsel, G. J. Mankey, and R. F. Willis, Phys. Rev. B **47**, 1540 (1993); J. E. Ortega, and F. J. Himpsel, Phys. Rev. Lett. **69**, 844 (1992).
[46]D. Pescia, D. Kerkmann, F. Schumann, and W. Gudat, Z. Phys. B **78**, 475 (1990); S. S. P. Parkin, R. Bhadra, and K. P. Roche, Phys. Rev. Lett. **66**, 2152 (1991); D. H. Mosca, F. Petroff, A. Fert, P. A. Schroeder, W. P. Pratt, Jr., and R. Laloee, J. Magn. Magn. Mater. **94**, L1 (1991).
[47]N. D. Mermin and H. Wagner, Phys. Rev. Lett. **17**, 1133 (1966).
[48]J. M. Kosterlitz and D. J. Thouless, J. Phys. C **6**, 1181 (1973); V. L. Berezinskii, Zh. Eksp. Teor. Fiz. **59**, 907 (1970) [Sov. Phys. JETP **32**, 493 (1971)].
[49]D. Pescia, M. Stanpanoni, G. L. Bona, A. Valerlaus, R. F. Willis, and F. Meier, Phys. Rev. Lett. **58**, 2126 (1987); C. Liu, E. R. Moog, and S. D. Bader, J. Appl. Phys. **64**, 5325 (1988); D. P. Papas, K. P. Kamper, and H. Hopster, Phys. Rev. Lett. **64**, 3179 (1990).
[50]V. L. Berezinski and A. Ya Blank, Zh. Eksp. Teor. Fiz. **64**, 725 (1973) [Sov. Phys. JETP **37**, 369 (1973)].
[51]J. V. José, L. P. Kadanoff, S. Kirkpatrick, and D. R. Nelson, Phys. Rev. B **16**, 1217 (1977).
[52]J. Tobochnik and G. V. Chester, Phys. Rev. B **20**, 3761 (1979).
[53]Z. Q. Qiu, J. Pearson, and S. D. Bader, Phys. Rev. Lett. **67**, 1646 (1991).
[54]R. Bergholz and U. Gradmann, J. Magn. Magn. Mater. **45**, 389 (1984).
[55]G. J. Mankey, R. F. Willis, and F. J. Himpsel, Phys. Rev. B **47**, 190 (1993).
[56]P. Krams, F. Lauks, R. L. Stamps, B. Hillebrands, and G. Güntherodt, Phys. Rev. Lett. **69**, 3674 (1992).

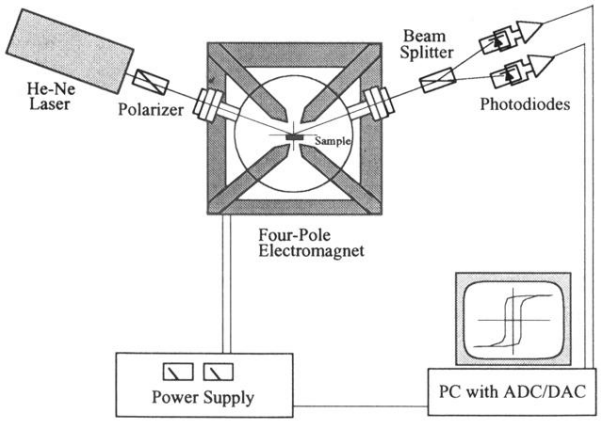

FIG. 1. Schematic diagram of the SMOKE apparatus.

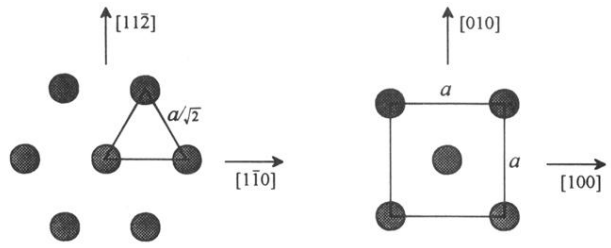

Cu(111) **Cu(100)**

FIG. 3. Unit cells of the Cu(111) and Cu(100) surfaces. The atomic area density is $2/a^2$ ($1/\text{Å}^2$) on Cu(100) and $4/(\sqrt{3}a^2)$ on Cu(111), $a = 3.61$ Å is the Cu lattice constant.